Journal of Power Sources 188 (2009) 367–378

Contents lists available at ScienceDirect

Journal of Power Sources

journal homepage: www.elsevier.com/locate/jpowsour

Comprehensive one-dimensional, semi-analytical, mathematical model for liquid-feed polymer electrolyte membrane direct methanol fuel cells

D. Kareemulla [1], S. Jayanti *

Department of Chemical Engineering, IIT-Madras, Chennai 600 036, Tamilnadu, India

ARTICLE INFO

Article history:
Received 5 August 2008
Received in revised form 11 November 2008
Accepted 19 November 2008
Available online 13 December 2008

Keywords:
Direct methanol fuel cell
Non-Tafel kinetics
Methanol crossover
Mixed potential effect
Mathematical modelling

ABSTRACT

Polymer electrolyte membrane direct methanol fuel cells (PEM-DMFCs) have several advantages over hydrogen-fuelled PEM fuel cells; but sluggish methanol electrochemical oxidation and methanol crossover from the anode to the cathode through the PEM are two major problems with these cells. In the present work, a comprehensive one-dimensional, single phase, isothermal mathematical model is developed for a liquid-feed PEM-DMFC, taking into account all the necessary mass transport and electrochemical phenomena. Diffusion and convective effects are considered for methanol transport on the anode side and in the PEM, whereas only diffusional transport of species is considered on the cathode side. A multi-step reaction mechanism is used to describe the electrochemical oxidation of methanol at the anode. Stefan–Maxwell equations are used to describe multi-component diffusion on the cathode side and Tafel type of kinetics is used to describe the simultaneous methanol oxidation and oxygen reduction reactions at the cathode. The model fully accounts for the mixed potential effect caused by methanol crossover at the cathode. It shows excellent agreement with literature data of the limiting current density for different low methanol feed concentrations at different operating temperatures. At high methanol feed concentrations, oxygen depletion on the cathode side, due to excessive methanol crossover, results in mass-transport limitations. The model can be used to optimize the geometric and physical parameters with a view to extracting the highest current density while still keeping a tolerably low methanol crossover.

1. Introduction

Diminishing fossil fuel reserves, ever escalating fuel prices, contemporary industrial developments and the rapid pace of urbanization call for secured and environmentally sustainable energy sources. Fuel cells are currently advocated as the most promising technology to meet our future energy requirements. They offer a potentially non-polluting and renewable means of generating electricity. Of the several types of fuel cell available today, liquid-feed polymer electrolyte membrane direct methanol fuel cells (PEM-DMFCs) have been extensively investigated in the past several years and are considered as leading contenders for transportation, portable and micro-power applications as they offer a combination of simplicity, robustness and high energy density [1–3]. Nevertheless, the commercial exploitation of liquid-feed PEM-DMFCs is being hindered by two major technical impediments, namely, sluggish electrochemical oxidation of methanol at the anode, which results in high anode overpotentials, and methanol crossover from the anode to the cathode through the PEM, which causes fuel and oxidant loss (on the anode and the cathode sides, respectively) and cathode electrode depolarization. A major breakthrough in the research and development of liquid-feed PEM-DMFCs has been the modification of platinum by a second component such as Pt–Ru. Even with this binary catalyst, however, the overpotential at the anode in a liquid-feed PEM-DMFC is still much higher than that of a hydrogen-fuelled PEMFCs.

To-date, even for an elaborately optimized PEM with reasonable ionic conductivity, methanol crossover is still a major challenge [4]. Many studies have been published in the literature dealing with the issue of methanol crossover, which is found to be strongly dependent on the methanol feed concentration. Constrained by the problem of methanol crossover, dilute methanol solutions (around 1.0 M) are usually employed in liquid-feed PEM-DMFCs. Although further dilution of methanol solutions will additionally reduce methanol crossover, mass transport limitation can become a serious problem and lead to lower limiting current densities, especially at methanol concentrations less than 0.5 M [5].

Besides the aforementioned phenomena, a variety of operating and geometric parameters affect the performance or polarization behaviour of liquid-feed PEM-DMFCs [6]. Comprehensive experimental investigations on fuel cells have traditionally been difficult and often turn out to be practically and economically unfeasible. Mathematical modelling has proved to be a potential

* Corresponding author. Tel.: +91 4422574168; fax: +91 4422570509.
E-mail address: sjayanti@iitm.ac.in (S. Jayanti).
[1] Currently at BPCL R&D Centre, Greater Noida, India.

0378-7753/$ – see front matter © 2008 Elsevier B.V. All rights reserved.
doi:10.1016/j.jpowsour.2008.11.138

tool in this regard to provide qualitative insights into the transport processes involved in fuel cells. Numerous models ranging from one-dimensional, single-phase [5,7–13] to multiphase, multidimensional [14–17] can be found in the literature. The majority of these models are primarily focused on overall cell polarization behaviour without systematically addressing important phenomena such as the mass transport-driven limiting current behaviour, the effect of some key parameters on methanol crossover and the consequent effect on the cell performance. Further, the physical domain is simplified by assuming the catalyst layers to be very thin and the mass-transport limitation on the cathode side is neglected. The electrochemical oxidation of methanol is described by Tafel kinetics with a fixed reaction order. In reality, this reaction is known to be a complex multi-step reaction which proceeds through a series of elementary reaction steps [18–20]. Recent experiments by Vidakovic et al. [21] show that the reaction order with respect to methanol to varies from zero (low overpotential, high concentrations) to close to unity (high overpotential, low concentrations). Therefore, a kinetic model must be employed that accurately accounts for the reaction order transition from zero to unity depending on the operating conditions.

In the present work, a comprehensive steady-state, isothermal, one-dimensional, single phase, semi-analytical mathematical model is developed taking into account all the necessary mass transport and electrochemical phenomena to predict the performance of a liquid-feed PEM-DMFC. The model also investigates the effect of key operating parameters on methanol crossover and methanol mass-transport-driven limiting current behaviour.

2. Mathematical model

A liquid-feed PEM-DMFC operates by the electrochemical oxidation of methanol and water at the anode in the presence of a Pt–Ru/C binary catalyst, i.e.,

$$CH_3OH + H_2O \rightarrow CO_2 + 6H^+ + 6e^- \quad (E^0_{anode} = 0.02\,V \text{ vs. SHE}) \tag{1}$$

and the electrochemical reduction of oxygen at the cathode in the presence of Pt/C catalyst:

$$\tfrac{3}{2}O_2 + 6H^+ + 6e^- \rightarrow 3H_2O \quad (E^0_{cathode} = 1.23\,V \text{ vs. SHE}) \tag{2}$$

The overall reaction can therefore be written as

$$CH_3OH + \tfrac{3}{2}O_2 \rightarrow CO_2 + 2H_2O \quad (E^0_{Cell} = 1.21\,V) \tag{3}$$

Fig. 1 depicts a schematic diagram of a liquid-feed PEM-DMFC segmented into seven regions, namely, anode flow chamber (AFC), anode backing layer (ABL), anode catalyst layer (ACL), polymer electrolyte membrane (PEM), cathode catalyst layer (CCL), cathode diffusion layer (CDL), and cathode flow chamber (CFC). The origin is set at the AFC|ABL interface. By convention, any flux in the direction of increasing thickness is taken to be positive. A summary of the species and the mass transport and/or electrochemical phenomena considered in each of these regions is presented in Table 1. The model is constructed based on the following assumptions.

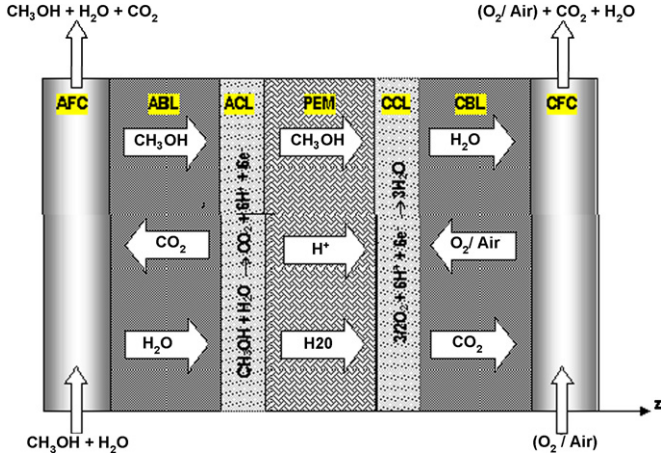

Fig. 1. Schematic division of a DMFC into seven regions.

Table 1
Species and phenomena considered in various regions of DMFC.

Region	Species considered	Mass transport	Electrochemical kinetics
AFC	Methanol, water, and dissolved carbon dioxide	√	
ABL	Methanol, water, and dissolved carbon dioxide	√	
ACL	Methanol and water	√	√ (non-Tafel type)
PEM	Methanol and water	√	
CCL	Oxygen	√	√ (Tafel type)
CDL	Oxygen, nitrogen, water vapor, and carbon dioxide	√	
CFC	Oxygen, nitrogen, water vapor, and carbon dioxide	√	

- The cell is operating under steady-state and isothermal conditions.
- Variations in only one spatial Cartesian co-ordinate, i.e., perpendicular to the membrane electrode assembly (MEA), are considered.
- The flow chambers are thoroughly mixed.
- The catalyst layers are macro-homogeneous porous electrodes. Therefore, the electrochemical reactions taking place in these regions are modelled as homogeneous reactions.
- CO_2 is fully dissolved and no CO_2 permeation takes place through the membrane.
- The membrane is assumed to be fully saturated.
- The electrolyte membrane is impervious to cathode side gases.
- Only water vapour is considered on the cathode side.
- The crossed-over methanol through the membrane is oxidized instantaneously at the PEM|CCL interface due to the large cathode overpotential imposed on the methanol.
- A voltage loss due to electronic resistance is not considered.
- The overpotential in the catalyst layer is ohmic in nature and since the catalyst layer is very thin, changes in overpotential are neglected.

The governing equations, for the each of the aforementioned regions, are described in detail in the following sub-sections.

2.1. Mass transport in the anode and cathode flow chambers

In the flow chambers, the reactants split their flow between the backing/diffusion layers and the channel exits, as determined by the reaction stoichiometry and the respective permeation rates. Since the contents in the flow chambers are thoroughly mixed, the concentration/mole fraction of the reactants at the flow-chamber|backing-layer interface is equal to the concentration/mole fraction of reactants in the exit stream, which can be determined by a mass balance of the species across the flow chambers, as described below. For liquid-phase transport in the AFC, a generalized mass balance over the anode-side species can be written as

$$n^{out}_{i,a} = n^{in}_{i,a} - A \times (N^{ABL}_i); \quad i = Me, W, C_1 \tag{4}$$

where $n^{in}_{i,a}$, $n^{out}_{i,a}$, N^{ABL}_i, and A represent the inlet and the outlet molar flow rates of species i on the anode side, the flux of species i through

the ABL, and the active area of the cell respectively. Now, since the concentration of methanol and dissolved carbon dioxide are very low in the anode-side exit stream, the mole fraction of methanol in the exit stream, x_{Me}^{out}, can be determined as

$$x_{Me}^{out} = \frac{C_{Me}^{out}}{C_W^{out} + C_{Me}^{out} + C_{C_1}^{out}} \approx \frac{C_{Me}^{out}}{C_W^{out}} = \frac{n_{Me,a}^{out}}{n_a^{out}} \quad (5)$$

where $n_{Me,a}^{Out}$ is the outlet molar flow rate of methanol on the anode side and n_a^{Out} is the total outlet molar flow rate on anode side, which is the sum of outlet flow rates of methanol, water and dissolved carbon dioxide calculated from Eq. (4).

From the last equality in Eq. (5), the concentration of methanol in the anode outlet stream, $C_{Me,a}^{out}$, which is assumed to be the concentration of methanol at the AFC|ABL interface, $C_{Me}^{AFC/ABL}$, can be expressed as

$$C_{Me,a}^{out} = C_{Me}^{AFC/ABL} = C_W^{out}\frac{n_{Me}^{out}}{n_a^{out}} = \left(\frac{\rho_W}{M_W}\right)\frac{n_{Me,a}^{out}}{n_a^{out}} \quad (6)$$

For gas phase transport in the CFC, a generalized mass balance over the cathode-side species can be written as

$$n_{i,c}^{out} = n_{i,c}^{in} - A \times (N_i^{CDL}); \quad i = O, N, WV, C_g \quad (7)$$

where $n_{i,c}^{in}$, $n_{i,c}^{out}$, N_i^{CDL} have the same meaning as before except that they pertain to the cathode side. Now, the mole fraction of each of these species in the exit stream, which is assumed to be the mole fraction at the CFC|CDL interface, can be determined as

$$x_{i,c}^{out} = x_i^{CFC/CDL} = \frac{n_{i,c}^{out}}{n_c^{out}} \quad (8)$$

where $n_{i,c}^{out}$ is the outlet molar flow rate of species i on cathode side, and n_c^{out} is the total molar flow rate, which is the sum of molar flow rates of oxygen, nitrogen, water vapour and carbon dioxide calculated from Eq. (7) on the cathode-side, respectively.

2.2. Mass transport in anode backing layer

A mixture of methanol, water and dissolved carbon dioxide are considered in this region. Dissolved carbon dioxide diffuses back into the AFC and exits with the solution. The flux of each of these species is composed of two factors: one required for the reaction and one that diffuses (crosses over) through the membrane. Therefore the flux in this region is expressed as

$$N_i^{ABL} = N_i^{Sto} + N_i^{PEM}; \quad i = Me, W, C_1 \quad (9)$$

where N_i^{Sto} and N_i^{PEM} represent the stoichiometric flux, i.e., flux required for the reaction and the flux diffusing through the PEM (crossover flux), respectively, of species i.

The stoichiometric flux is determined by the reaction stoichiometry:

$$N_{Me}^{Sto} = N_W^{Sto} = -N_{C_1}^{Sto} = \frac{I}{6F} \quad (10)$$

where I is the cell current density and F is the Faraday constant (96, 485 C mol^{-1}). As assumed earlier, the crossover flux of dissolved carbon dioxide is set to zero. Methanol transport in this region is a combination of diffusion and convection. Therefore, the flux of methanol, N_{Me}^{ABL}, is expressed as

$$N_{Me}^{ABL} = -D_{Me-W}^{ABL,eff}\frac{dC_{Me}^{ABL}}{dz} + x_{Me}^{ABL}N_{Tot}^{ABL} \quad (11)$$

where x_{Me}^{ABL}, N_{Tot}^{ABL} are the local mole fraction of methanol in the ABL, and total flux through the ABL, respectively. Here

$$N_{Tot}^{ABL} = N_{Me}^{ABL} + N_W^{ABL} + N_{C_1}^{ABL} \quad (12)$$

$D_{Me-W}^{ABL,eff}$ is the effective diffusivity coefficient of methanol in water in the ABL and is given by

$$D_{Me-W}^{ABL,eff} = (\varepsilon^{ABL})^{1.5} D_{Me-W}$$

where ε^{ABL} is the porosity of the ABL, the exponent 1.5 is the Bruggeman correction factor that accounts for pore tortuosity, and D_{Me-W} is the diffusivity coefficient of methanol in water.

Since the concentrations of methanol and dissolved carbon dioxide are very low, Eq. (11) can be written as

$$N_{Me}^{ABL} = -D_{Me}^{ABL,eff}\frac{dC_{Me}^{ABL}}{dz} + \nu_s^{ABL}C_{Me}^{ABL} \quad (13)$$

where $\nu_s^{ABL} = (M_W/\rho_W)N_{Tot}^{ABL}$ is the superficial convective velocity in the ABL; M_W and ρ_W are molecular weight and density of water, respectively.

Since there is no chemical reaction in this region, the flux of any species remains constant. Thus,

$$\frac{dN_i^{ABL}}{dz} = 0; \quad i = Me, W, C_1 \quad (14)$$

Writing down Eq. (14) for methanol and combining with Eq. (11), the following implicit expression for methanol flux through the ABL, N_{Me}^{ABL}, can be obtained as

$$N_{Me}^{ABL} = \frac{C_{Me}^{AFC/ABL}\exp(\nu_s^{ABL}/k^{ABL}) - C_{Me}^{ABL/ACL}}{\exp(\nu_s^{ABL}/k^{ABL}) - 1}\nu_s^{ABL} \quad (15)$$

where $k^{ABL} = D_{Me}^{ABL,eff}/\delta^{ABL}$ is the mass transfer coefficient of methanol in the ABL, δ^{ABL} is the thickness of the ABL, and $C_{Me}^{ABL/ACL}$ is the concentration of methanol at the ABL|ACL interface.

2.3. Mass transport and electrochemical phenomena in the anode catalyst layer

2.3.1. Mass transport in anode catalyst layer

A fraction of the methanol solution, arrived in this region through the ABL, gets electrochemically oxidized in the presence of Pt–Ru/C catalyst via the electrochemical reaction shown in Eq. (1) and the rest is transported through the PEM by different driving forces depending upon the operating conditions.

A binary mixture of methanol and water is considered in this region and the flux of each of these species is assumed to vary linearly as

$$N_{Me}^{ACL} = N_{Me}^{ABL} - \frac{I}{6F}\left[\frac{z - z^{ABL/ACL}}{\delta^{ACL}}\right] \quad (16)$$

$$N_W^{ACL} = N_W^{ABL} - \frac{I}{6F}\left[\frac{z - z^{ABL/ACL}}{\delta^{ACL}}\right] \quad (17)$$

where δ^{ACL} is the thickness of the ACL.

Therefore, the total flux variation in the ACL, N_{Tot}^{ACL}, is given by

$$N_{Tot}^{ACL} = N_{Tot}^{ABL} - \frac{I}{3F}\left[\frac{z - z^{ABL/ACL}}{\delta^{ACL}}\right] \quad (18)$$

Methanol transport in this layer is a combination of diffusion and convection. Therefore, the flux of methanol in this region N_{Me}^{ACL} is expressed as

$$N_{Me}^{ACL} = -D_{Me-W}^{ACL,eff}\frac{dC_{Me}^{ACL}}{dz} + \overline{N_{Tot}^{ACL}}x_{Me}^{ACL} \quad (19)$$

where $\overline{N_{Tot}^{ACL}}$ is the averaged total flux obtained from Eq. (17) and $D_{Me-W}^{ACL,eff}$ is the effective diffusivity coefficient of methanol in water

in the ACL and is given by

$$D_{\mathrm{Me-W}}^{\mathrm{ACL,eff}} = \left(\varepsilon^{\mathrm{ACL}}\right)^{1.5} D_{\mathrm{Me-W}}$$

where $\varepsilon^{\mathrm{ACL}}$ is the porosity of the ACL.

Eq. (19) can be further written as

$$N_{\mathrm{Me}}^{\mathrm{ACL}} = -D_{\mathrm{Me-W}}^{\mathrm{ACL,eff}} \frac{\mathrm{d}C_{\mathrm{Me}}^{\mathrm{ACL}}}{\mathrm{d}z} + \overline{v_{\mathrm{s}}^{\mathrm{ACL}}} C_{\mathrm{Me}}^{\mathrm{ACL}} \tag{20}$$

where $\overline{v_{\mathrm{s}}^{\mathrm{ACL}}} = (M_{\mathrm{W}}/\rho_{\mathrm{W}})\overline{N_{\mathrm{Tot}}^{\mathrm{ACL}}}$ is the average superficial convective velocity in the ACL.

Equating Eqs. (16) and (20) and upon solving with the boundary condition $C_{\mathrm{Me}}^{\mathrm{ACL}} = C_{\mathrm{Me}}^{\mathrm{ABL/ACL}}$ at $z = z^{\mathrm{ABL/ACL}}$, the following expression for the distribution of methanol concentration in the ACL, $C_{\mathrm{Me}}^{\mathrm{ACL}}(z)$, can be obtained, i.e.,

$$C_{\mathrm{Me}}^{\mathrm{ACL}}(z) = C_{\mathrm{Me}}^{\mathrm{ABL/ACL}} + \left(\frac{\overline{v_{\mathrm{s}}^{\mathrm{ACL}}}}{D_{\mathrm{Me-W}}^{\mathrm{ACL,eff}}} C_{\mathrm{Me}}^{\mathrm{ABL/ACL}} - \frac{N_{\mathrm{Me}}^{\mathrm{ABL}}}{D_{\mathrm{Me-W}}^{\mathrm{ACL,eff}}} \right) (z - z^{\mathrm{ABL/ACL}}) \tag{21}$$

2.3.2. Kinetic model for methanol electrochemical oxidation in anode catalyst layer

A simplified Gasteiger mechanism [22] is used in the present work to develop a kinetic expression similar to that of Meyers and Newman [23] describing the reaction rate of methanol in terms of methanol concentration and the anode overpotential, and is later on used to obtain anode overpotential data. The reaction mechanism consists of the following elementary steps:

$$\mathrm{CH_3OH_{AFC}} \rightarrow \mathrm{CH_3OH_{ACL}} \quad \text{(mass transfer)} \tag{22a}$$

$$\mathrm{CH_3OH + Pt} \rightarrow \mathrm{CH_3OH_{ad,Pt}} \rightarrow \cdots \mathrm{CO_{ad,Pt} + 4H^+ + 4e^-} \tag{22b}$$

$$\mathrm{H_2O + Ru} \Leftrightarrow \mathrm{OH_{ad,Ru} + H^+ + e^-} \tag{22c}$$

$$\mathrm{CO_{ad,Pt} + OH_{ad,Ru}} \rightarrow \mathrm{CO_2 + H^+ + e^- + Pt + Ru} \tag{22d}$$

As a first step (22a), methanol is transferred from the AFC, through the ABL, into the ACL wherein the electrochemical oxidation of methanol takes place through several steps. The potential-dependent final step (22d) involving the reaction between two surface-adsorbed species is the rate-determining step, except at sufficiently high current densities, where the first step (potential-independent methanol physiosorption) of the consecutive irreversible reaction sequence (22b) limits the reaction. The third step (22c), i.e., the water dissociative adsorption, is assumed to be in equilibrium.

The balance of adsorbed species on the surface of the two catalyst components, platinum and ruthenium, yields:

$$\theta_{\mathrm{Pt}} + \theta_{\mathrm{C,Pt}} = 1 \tag{23a}$$

where $\theta_{\mathrm{C,Pt}}$ refers to fractional coverage on Pt by some C-containing adsorbates without specifying the type of the adsorbed species. Similarly:

$$\theta_{\mathrm{Ru}} + \theta_{\mathrm{OH,Ru}} = 1 \tag{23b}$$

The rate expressions for every step considered in the above mechanism are formulated as follows. The rate expression for the reaction step (22b) is written as

$$r_1 = k_1 C_{\mathrm{Me}} \theta_{\mathrm{Pt}} \tag{24}$$

where r_1 and k_1 represent the rate of reaction and the reaction rate constant of step (22b), respectively.

From Eqs. (23a) and (24), we have

$$r_1 = k_1 C_{\mathrm{Me}} (1 - \theta_{\mathrm{C,Pt}}) \tag{25}$$

For the reaction step (22c), the rate expression is written as

$$r_2 = k_{2,\mathrm{f}} a_{\mathrm{W}} \theta_{\mathrm{Ru}} \exp\left[\frac{\alpha_2 F V_{\mathrm{a}}}{RT}\right] - k_{2,\mathrm{b}} \theta_{\mathrm{OH,Ru}} \exp\left[\frac{-(1-\alpha_2) F V_{\mathrm{a}}}{RT}\right] \tag{26}$$

where r_2, $k_{2,\mathrm{f}}$, $k_{2,\mathrm{b}}$, and α_2 represent the rate of reaction, the forward and the backward chemical reaction rate constants, and the transfer coefficient of step (22c), respectively, and V_{a} is the anode voltage.

From Eqs. (23b) and (26), we have

$$r_2 = k_{2,\mathrm{a}} a_{\mathrm{W}} (1 - \theta_{\mathrm{OH,Ru}}) \exp\left[\frac{\alpha_2 F V_{\mathrm{a}}}{RT}\right] - k_{2,\mathrm{b}} \theta_{\mathrm{OH,Ru}} \exp\left[\frac{-(1-\alpha_2) F V_{\mathrm{a}}}{RT}\right] \tag{27}$$

where a_{W} is the activity of water.

As this reaction is assumed to be in equilibrium, Eq. (27) can be solved for $\theta_{\mathrm{OH,Ru}}$ as (water activity, a_{W} is unity):

$$\theta_{\mathrm{OH,Ru}} = \frac{K_2 \exp(F V_{\mathrm{a}}/RT)}{1 + K_2 \exp(F V_{\mathrm{a}}/RT)} \tag{28}$$

where $K_2 = k_{2,\mathrm{f}}/k_{2,\mathrm{b}}$ is the chemical equilibrium constant of reaction step (22c).

For the reaction step (22d), the rate expression is written as

$$r_3 = k_3 \theta_{\mathrm{C,Pt}} \theta_{\mathrm{OH,Ru}} \exp\left[\frac{\alpha_3 F V_{\mathrm{a}}}{RT}\right] \tag{29}$$

where r_3, k_3 and α_3 represent the rate of reaction, the chemical reaction rate constant and the transfer coefficient of step (22d), respectively.

Applying steady-state conditions, i.e., $r_1 = r_3$, one can obtain an expression for $\theta_{\mathrm{C,Pt}}$ as

$$\theta_{\mathrm{C,Pt}} = \frac{k_1 C_{\mathrm{Me}} (1 + K_2 \exp(F V_{\mathrm{a}}/RT))}{k_3 K_2 \exp((\alpha_3 + 1) F V_{\mathrm{a}}/RT) + k_1 C_{\mathrm{Me}} (1 + K_2 \exp(F V_{\mathrm{a}}/RT))} \tag{30}$$

Now, the overall reaction rate can be expressed by either the rate of reaction of step (22b), or by the rate of reaction of step (22d). Since six electrons are exchanged in the oxidation reaction, the corresponding anodic current density, j_{a}, can be obtained as

$$j_{\mathrm{a}} = 6F r_3 = 6F k_3 \theta_{\mathrm{C,Pt}} \theta_{\mathrm{OH,Ru}} \exp\left[\frac{\alpha_3 F V_{\mathrm{a}}}{RT}\right] \tag{31}$$

Combining Eqs. (27), (29) and (30) and assuming $K_2 \exp(FV/RT) \gg 1$, we get for the anodic current density the following expression:

$$j_{\mathrm{a}} = 6F \frac{k_3 C_{\mathrm{Me}} \exp(\alpha_3 F V_{\mathrm{a}}/RT)}{C_{\mathrm{Me}} + (k_3/k_1) \exp(\alpha_3 F V_{\mathrm{a}}/RT)} \tag{32}$$

Replacing α_3 by α_{a}, the anodic current density given in Eq. (32) can be further expressed in terms of anode overpotential as

$$j_{\mathrm{a}} = \frac{\beta C_{\mathrm{Me}} \exp(\alpha_{\mathrm{a}} \eta_{\mathrm{a}} F/RT)}{C_{\mathrm{Me}} + \gamma \exp(\alpha_{\mathrm{a}} F \eta_{\mathrm{a}}/RT)} \tag{33}$$

The kinetic parameters appearing in Eq. (33), namely, β and γ, are given by

$$\beta = 6F k_3 \exp\left(\frac{\alpha_{\mathrm{a}} F E_{\mathrm{a}}}{RT}\right)$$

$$\gamma = \frac{k_3}{k_1} \exp\left(\frac{\alpha_{\mathrm{a}} F E_{\mathrm{a}}}{RT}\right)$$

where E_{a} is the equilibrium anode potential.

The transition of the reaction order from zero, at low overpotentials (the second term in the denominator of Eq. (33) can be ignored, i.e., the reaction is potential dependent), to one at high overpotentials (concentration of methanol becomes low; therefore the first term in the denominator of Eq. (33) can be ignored, i.e., the reaction is concentration dependent) can be observed from Eq. (33).

Integration of Eq. (33) over the anode catalyst layer yields the cell current density, I, as

$$I = \int_0^{\delta_{ACL}} \frac{\beta C_{Me}^{ACL}(z)\exp(\alpha_a \eta_a F/RT)}{C_{Me}^{ACL}(z) + \gamma \exp(\alpha_a F \eta_a/RT)}\, dz \quad (34)$$

This kinetic expression along with Eq. (21) is used to calculate the anode overpotential for any given cell current density.

2.4. Mass transport in polymer electrolyte membrane

Following the approach of Bernardi and Verbrugge [24], the Nernst–Planck equation with the modified Schlogl equation is used to characterize the transport of species in the membrane electrolyte region:

$$N_i^{PEM} = -Z_i^{PEM}\frac{F}{RT}D_i^{PEM}C_i^{PEM}\frac{d\phi}{dz} - D_i^{PEM}\frac{dC_i^{PEM}}{dz} + C_i^{PEM}v^{PEM} \quad (35)$$

In accordance with the modified Schlogl equation, the pore convective velocity, v^{PEM}, is given by

$$v^{PEM} = \frac{k_\Phi}{\mu}Z_f^{PEM}C_f^{PEM}F\frac{d\phi}{dz} - \frac{k_p}{\mu}\frac{dP}{dz} \quad (36)$$

where k_Φ is the electrokinetic permeability, C_f^{PEM} is the concentration of fixed charge species (sulfonic acid groups) in the PEM, Z_f^{PEM} is the charge number of fixed charge species in the PEM, k_p is the hydraulic permeability, and μ is the liquid water viscosity.

For neutral species, the first term of Eq. (35) vanishes. Therefore, the superficial flux of neutral species in the membrane electrolyte region is expressed as

$$N_i^{PEM} = -D_{i,eff}^{PEM}\frac{dC_i^{PEM}}{dz} + C_i^{PEM}v_s^{PEM}; \quad i = Me, W \quad (37)$$

where v_s^{PEM} is the superficial convective velocity in the membrane and is given by

$$v_s^{PEM} = \varepsilon_W^{PEM}v^{PEM}$$

Here ε_W^{SPEM} is the volume fraction of water in the PEM which is given by

$$\varepsilon_W^{PEM} = \frac{\lambda}{(\bar{V}^{PEM}/\bar{V}_W) + \lambda}$$

where $\bar{V}^{PEM}$, $\bar{V}_W$ and λ are the partial molar volume of the membrane, the partial molar volume of water and the membrane water loading or water content, respectively.

The equivalent weight (EW) of the membrane (grams of dry polymer/moles of sulfonic acid groups) and $\bar{V}^{PEM}$ are interrelated:

$$\bar{V}^{PEM} \approx \frac{EW}{\rho_0}$$

where ρ_0 is the density of the dry membrane. For Nafion® 117, 115, or 112, the membranes of interest here, EW = 1100, and $\rho_0 = 2050\ kg\ m^{-3}$. The water uptake values of Nafion from liquid water determined by Hinatsu et al. [25] are used in the present work.

As no chemical reaction takes place, the flux of methanol and water remain constant:

$$\frac{dN_i^{PEM}}{dz} = 0; \quad i = Me, W \quad (38)$$

Inserting Eq. (36) into Eq. (35) and by applying it for proton transport, an expression for the potential gradient across the PEM, $d\phi/dz$, can be formulated in terms of two known parameters, namely, cell current density, I, and pressure gradient across the PEM, dp/dz, as shown in Eq. (39):

$$\frac{d\phi}{dz} = -\frac{(I/F) + C_{H^+}^{PEM}(k_p/\mu)(dP/dz)}{FC_{H^+}^{PEM}((D_{H^+}^{PEM}/RT) + (k_\Phi/\mu)C_{H^+}^{PEM})} \quad (39)$$

Substituting Eq. (39) in Eq. (36), an explicit expression for the pore convective velocity in the PEM, v^{PEM}, can be derived as

$$v^{PEM} = \frac{k_\Phi}{\mu}\left[\frac{(I/F) + C_{H^+}^{PEM}(k_p/\mu)(dp/dz)}{((D_{H^+}^{PEM}/RT) + (k_\Phi/\mu)C_{H^+}^{PEM})}\right] - \frac{k_p}{\mu}\frac{dp}{dz} \quad (40)$$

Water transport across the PEM takes place via diffusion and convection. Since the membrane is assumed to be fully saturated, only convective water transport is considered. Therefore, the flux of water across the PEM, N_W^{PEM}, is given by

$$N_{Me}^{PEM} = C_W^{PEM}v_s^{PEM} = \frac{v_s^{PEM}}{\bar{V}_W} \quad (41)$$

Methanol is transported through the PEM in the same way as it is transported through the ABL. So, the flux of methanol through the PEM or the crossover flux of methanol can be expressed in a similar form, as shown in Eq. (15). However, since the crossed-over methanol is assumed to be instantaneously oxidized at the PEM|CCL interface, this equation can be further reduced to the form shown in Eq. (42) by setting the concentration of methanol at the PEM/CCL, $C_{Me}^{ACL/PEM}$, equal to zero:

$$N_{Me}^{PEM} = \frac{C_{Me}^{ACL/PEM}\exp(v_s^{PEM}/k^{PEM})}{\exp(v_s^{PEM}/k^{PEM}) - 1}v_s^{PEM} \quad (42)$$

Six protons and six electrons are released for each mole of methanol consumed by the cathodic methanol oxidation reaction. Therefore the crossover current density, I^{Cross}, can be calculated by multiplying N_{Me}^{PEM} by a factor of 6F, as shown in Eq. (43):

$$I^{Cross} = 6FN_{Me}^{PEM} \quad (43)$$

Once the crossover current density is calculated, the methanol crossover efficiency and the Faradaic or fuel utilization efficiency, I^{Cross} and $I^{Fardaic}$, respectively, can be calculated in percentage terms as follows:

$$I^{Cross}\ (\%) = 100\frac{I^{Cross}}{I + I^{Cross}} \quad (44)$$

$$I^{Fardaic}\ (\%) = 100\frac{I}{I + I^{Cross}} \quad (45)$$

2.5. Mass transport in cathode diffusion layer

The gas phase in the CDL of a liquid-feed PEM-DMFC is a mixture of oxygen, nitrogen (if air is used as cathode feed), carbon dioxide, and water vapour. The gaseous mixture is assumed to be an ideal gas. Only diffusional effects are considered in this region and the Stefan–Maxwell equations are used to account for multicomponent diffusion. For the diffusion of an n-component ideal gas through a porous medium, the one-dimensional Stefan–Maxwell equations take the form:

$$\frac{dx_i^{CDL}}{dz} = \sum_{j=1}^{n}\frac{1}{cD_{i-j}^{eff}}(x_i^{CDL}N_j^{CDL} - x_j^{CDL}N_i^{CDL}); \quad i = 1, 2, \ldots, n \quad (46)$$

where cD_{i-j}^{eff} is the effective concentration binary diffusion coefficient and is given by

$$cD_{i-j}^{CDL,eff} = (\varepsilon^{CDL})^{1.5}cD_{i-j}$$

where cD_{i-j} is the concentration binary diffusivity coefficient and ε^{CDL} is the porosity of the CBL.

Nitrogen does not participate in any of the chemical reactions; it is inert. Therefore, under steady-state conditions, it remains motionless and hence its flux is set to be zero:

$$N_{\mathrm{N}}^{\mathrm{CDL}} = 0 \tag{47}$$

The fluxes of the other three species are obtained as described below.

The flux of oxygen in this region is made up of two factors: the flux required for the cathode half-cell reaction and that required for the complete oxidation of the crossed-over methanol. Therefore, the flux of oxygen through the CDL, $N_{\mathrm{O}}^{\mathrm{CDL}}$, and is given by

$$N_{\mathrm{O}}^{\mathrm{CDL}} = -\left(\frac{I}{4F} + \frac{3}{2}N_{\mathrm{Me}}^{\mathrm{PEM}}\right) \tag{48}$$

Only water in vapour form is considered in this region. The flux of water vapour is made up of three factors: the flux produced by the cathode half-cell reaction, that produced by the complete oxidation of the crossed-over methanol, and the flux of water through the PEM, $N_{\mathrm{W}}^{\mathrm{PEM}}$. Therefore, the flux of water vapour through the CDL, $N_{\mathrm{WV}}^{\mathrm{CDL}}$, is given by

$$N_{\mathrm{WV}}^{\mathrm{CDL}} = \frac{I}{3F} + 2N_{\mathrm{Me}}^{\mathrm{PEM}} + N_{\mathrm{W}}^{\mathrm{PEM}} \tag{49}$$

One mole of carbon dioxide will be formed for every mole of crossed-over methanol consumed. Therefore, the flux of carbon dioxide through the CDL, $N_{C_g}^{\mathrm{CDL}}$, is given by

$$N_{C_g}^{\mathrm{CDL}} = N_{\mathrm{Me}}^{\mathrm{PEM}} \tag{50}$$

Since no chemical reaction occurs in this region, the flux of each of these species remains constant leading to

$$\frac{\mathrm{d}N_i^{\mathrm{CDL}}}{\mathrm{d}z} = 0; \quad i = \mathrm{O}, \mathrm{WV}, C_g \tag{51}$$

Applying Eq. (46) for nitrogen (N), oxygen (O) and water vapour (WV), the following set of linear differential equations can be obtained:

$$\frac{\mathrm{d}x_{\mathrm{N}}^{\mathrm{CDL}}}{\mathrm{d}z} = \left[\frac{N_{\mathrm{O}}^{\mathrm{CDL}}}{cD_{\mathrm{N-O}}^{\mathrm{eff}}} + \frac{N_{\mathrm{WV}}^{\mathrm{CDL}}}{cD_{\mathrm{N-W}}^{\mathrm{eff}}} + \frac{N_{C_g}^{\mathrm{CDL}}}{cD_{\mathrm{N-C}}^{\mathrm{eff}}}\right] x_{\mathrm{N}}^{\mathrm{CDL}} \tag{52a}$$

$$\begin{aligned}\frac{\mathrm{d}x_{\mathrm{O}}^{\mathrm{CDL}}}{\mathrm{d}z} = {} & \left(\frac{N_{\mathrm{O}}^{\mathrm{CDL}}}{cD_{\mathrm{O-C}}^{\mathrm{eff}}} + \frac{N_{\mathrm{WV}}^{\mathrm{CDL}}}{cD_{\mathrm{O-W}}^{\mathrm{eff}}} + \frac{N_{C_g}^{\mathrm{CDL}}}{cD_{\mathrm{O-C}}^{\mathrm{eff}}}\right) x_{\mathrm{O}}^{\mathrm{CBL}} \\ & + \left(\frac{N_{\mathrm{O}}^{\mathrm{CDL}}}{cD_{\mathrm{O-C}}^{\mathrm{eff}}} - \frac{N_{\mathrm{O}}^{\mathrm{CDL}}}{cD_{\mathrm{O-W}}^{\mathrm{eff}}}\right) x_{\mathrm{WV}}^{\mathrm{CDL}} \\ & + \left(\frac{N_{\mathrm{O}}^{\mathrm{CDL}}}{cD_{\mathrm{O-C}}^{\mathrm{eff}}} - \frac{N_{\mathrm{O}}^{\mathrm{CDL}}}{cD_{\mathrm{O-N}}^{\mathrm{eff}}}\right) x_{\mathrm{N}}^{\mathrm{CDL}} - \frac{N_{\mathrm{O}}^{\mathrm{CDL}}}{cD_{\mathrm{O-C}}^{\mathrm{eff}}}\end{aligned} \tag{52b}$$

$$\begin{aligned}\frac{\mathrm{d}x_{\mathrm{WV}}^{\mathrm{CDL}}}{\mathrm{d}z} = {} & \left(\frac{N_{\mathrm{O}}^{\mathrm{CDL}}}{cD_{\mathrm{WV-O}}^{\mathrm{eff}}} + \frac{N_{\mathrm{WV}}^{\mathrm{CDL}}}{cD_{\mathrm{WV-C}}^{\mathrm{eff}}} + \frac{N_{C_g}^{\mathrm{CDL}}}{cD_{\mathrm{WV-C}}^{\mathrm{eff}}}\right) x_{\mathrm{WV}}^{\mathrm{CDL}} \\ & + \left(\frac{N_{\mathrm{WV}}^{\mathrm{CDL}}}{cD_{\mathrm{WV-C}}^{\mathrm{eff}}} - \frac{N_{\mathrm{WV}}^{\mathrm{CDL}}}{cD_{\mathrm{WV-O}}^{\mathrm{eff}}}\right) x_{\mathrm{O}}^{\mathrm{CDL}} \\ & + \left(\frac{N_{\mathrm{WV}}^{\mathrm{CDL}}}{cD_{\mathrm{WV-C}}^{\mathrm{eff}}} - \frac{N_{\mathrm{WV}}^{\mathrm{CDL}}}{cD_{\mathrm{WV-N}}^{\mathrm{eff}}}\right) x_{\mathrm{N}}^{\mathrm{CBL}} - \frac{N_{\mathrm{WV}}^{\mathrm{CDL}}}{cD_{\mathrm{WV-C}}^{\mathrm{eff}}}\end{aligned} \tag{52c}$$

Eqs. (52a)–(52c) can be solved analytically for the species concentration distributions across the CDL, and the resulting equations are given in Eqs. (53a)–(53c).

$$x_{\mathrm{O}}^{\mathrm{CDL}}(z) = c_1 \exp(m_1 z) + c_2 \exp(m_2 z) + E_1 x_{\mathrm{N}}^{\mathrm{CDL}}(z) + E_2 \tag{53a}$$

$$\begin{aligned}x_{\mathrm{WV}}^{\mathrm{CBL}}(z) = {} & \frac{c_1}{B_1}(m_1 - A_1)\exp(m_1 z) + \frac{c_2}{B_1}(m_2 - A_1)\exp(m_2 z) \\ & + \left[\frac{E_1(K_1 - A_1) - C_1}{B_1}\right] x_{\mathrm{N}}^{\mathrm{CBL}}(z) + \frac{N_{\mathrm{O}}^{\mathrm{CBL}}}{B_1 cD_{\mathrm{O-C}}^{\mathrm{eff}}} - \frac{A_1 E_2}{B_1}\end{aligned} \tag{53b}$$

where

$$x_{\mathrm{N}}^{\mathrm{CDL}}(z) = x_{\mathrm{N}}^{\mathrm{CDL/CFC}} \exp(K_1(z - z^{\mathrm{CDL/CFC}})) \tag{53c}$$

The constants appearing in the above equations are given below:

$$A_1 = \left(\frac{N_{\mathrm{O}}^{\mathrm{CDL}}}{cD_{\mathrm{O-C}}^{\mathrm{eff}}} + \frac{N_{\mathrm{WV}}^{\mathrm{CDL}}}{cD_{\mathrm{O-WV}}^{\mathrm{eff}}} + \frac{N_{C_g}^{\mathrm{CDL}}}{cD_{\mathrm{O-C}}^{\mathrm{eff}}}\right);$$

$$A_2 = \left(\frac{N_{\mathrm{WV}}^{\mathrm{CDL}}}{cD_{\mathrm{WV\text{-}C}}^{\mathrm{eff}}} - \frac{N_{\mathrm{WV}}^{\mathrm{CDL}}}{cD_{\mathrm{WV-O}}^{\mathrm{eff}}}\right)$$

$$B_1 = \left(\frac{N_{\mathrm{O}}^{\mathrm{CDL}}}{cD_{\mathrm{O-C}}^{\mathrm{eff}}} - \frac{N_{\mathrm{O}}^{\mathrm{CDL}}}{cD_{\mathrm{O-WV}}^{\mathrm{eff}}}\right);$$

$$B_2 = \left(\frac{N_{\mathrm{O}}^{\mathrm{CDL}}}{cD_{\mathrm{WV-O}}^{\mathrm{eff}}} + \frac{N_{\mathrm{WV}}^{\mathrm{CDL}}}{cD_{\mathrm{WV-C}}^{\mathrm{eff}}} + \frac{N_{C_g}^{\mathrm{CDL}}}{cD_{\mathrm{WV-C}}^{\mathrm{eff}}}\right)$$

$$C_1 = \left(\frac{N_{\mathrm{O}}^{\mathrm{CDL}}}{cD_{\mathrm{O\text{-}C}}^{\mathrm{eff}}} - \frac{N_{\mathrm{O}}^{\mathrm{CDL}}}{cD_{\mathrm{O-N}}^{\mathrm{eff}}}\right); \qquad C_2 = \left(\frac{N_{\mathrm{WV}}^{\mathrm{CDL}}}{cD_{\mathrm{WV-C}}^{\mathrm{eff}}} - \frac{N_{\mathrm{WV}}^{\mathrm{CDL}}}{cD_{\mathrm{WV-N}}^{\mathrm{eff}}}\right)$$

$$K_1 = \left[\frac{N_{\mathrm{O}}^{\mathrm{CDL}}}{cD_{\mathrm{N-O}}^{\mathrm{eff}}} + \frac{N_{\mathrm{WV}}^{\mathrm{CDL}}}{cD_{\mathrm{N-WV}}^{\mathrm{eff}}} + \frac{N_{C_g}^{\mathrm{CDL}}}{cD_{\mathrm{N-C}}^{\mathrm{eff}}}\right];$$

$$E_1 = \frac{(C_1 K_1 - B_2 C_1 + B_1 C_2)}{K_1^2 - (A_1 + B_2)K_1 + (A_1 B_2 - A_2 B_1)}$$

$$E_2 = \frac{(N_O^{CDL} B_2 / cD_{O-C}^{eff}) - (N_{\mathrm{WV}}^{\mathrm{CDL}} B_1 / cD_{\mathrm{WV-C}}^{\mathrm{eff}})}{A_1 B_2 - A_2 B_1};$$

$$(m_1, m_2) = \frac{(A_1 + B_2) \pm \sqrt{(A_1 + B_2)^2 - 4(A_1 B_2 - A_2 B_1)}}{2}$$

$$c_1 = \frac{\begin{array}{c}(m_2 - A_1)x_{\mathrm{O}}^{\mathrm{CDL/CFC}} - B_1 x_{\mathrm{W}}^{\mathrm{CDL/CFC}} - (E_1 m_2 - E_1 K_1 + C_1)x_{\mathrm{N}}^{\mathrm{CDL/CFC}} \\ -E_2 m_2 + (N_{\mathrm{O}}^{\mathrm{CDL}}/cD_{\mathrm{O-C}}^{\mathrm{eff}})\end{array}}{(m_2 - m_1)\exp(m_1 z^{\mathrm{CDL/CFC}})}$$

$$c_2 = \frac{\begin{array}{c}(m_1 - A_1)x_{\mathrm{O}}^{\mathrm{CDL/CFC}} - B_1 x_{\mathrm{W}}^{\mathrm{CDL/CFC}} - (E_1 m_1 - E_1 K_1 + C_1)x_{\mathrm{N}}^{\mathrm{CDL/CFC}} \\ -E_2 m_1 + (N_{\mathrm{O}}^{\mathrm{CDL}}/cD_{\mathrm{O-C}}^{\mathrm{eff}})\end{array}}{(m_1 - m_2)\exp(m_2 z^{\mathrm{CDL/CFC}})}$$

The binary concentration diffusivity coefficients, cD_{i-j} are estimated using the following correlation [26]:

$$cD_{\mathrm{AB}} = 2.2646 \times 10^{-5} \sqrt{T\left(\frac{1}{M_{\mathrm{A}}} + \frac{1}{M_{\mathrm{B}}}\right)} \frac{1}{\sigma_{\mathrm{AB}}^2 \Omega_{\mathrm{D,AB}}}$$

The dimensionless quantity $\Omega_{\mathrm{D,AB}}$ – the "Collisional integral" for diffusion – is a function of the dimensionless temperature $KT/\varepsilon_{\mathrm{AB}}$. The collision integrals have been curve fitted by Neufeld et al. [27] as follows:

$$\begin{aligned}\Omega_{\mathrm{D,AB}} = {} & \frac{1.06036}{T^{*0.15610}} + \frac{0.19300}{\exp(0.47635T^*)} + \frac{1.03587}{\exp(1.52996T^*)} \\ & + \frac{1.76474}{\exp(3.89411T^*)}\end{aligned}$$

where $T^* = KT/\varepsilon_{\mathrm{AB}}$.

Here, $\varepsilon_{AB} = \sqrt{\varepsilon_A \varepsilon_B}$ and $\sigma_{AB} = (1/2)(\sigma_A + \sigma_B)$ are the molecular separation at collision and the energy of molecular attraction respectively [28].

2.6. Mass transport and electrochemical phenomena in cathode catalyst layer

2.6.1. Mass transport in cathode catalyst layer

Oxygen transport in this region is governed by diffusion. Therefore the flux of oxygen in this region, N_O^{CCL}, is given by Fick's law as

$$N_O^{CCL} = D_O^{CCL,eff} \frac{dC_O^{CCL}}{dz} \tag{54}$$

where $D_O^{CCL,eff}$ is the effective diffusion coefficient of oxygen in the CCL and is given by

$$D_O^{CCL,eff} = \left(\varepsilon^{CCL}\right)^{1.5} D_O^{CCL}$$

where ε^{CCL} is the porosity of the CCL and D_O^{CCL} is the diffusivity coefficient of oxygen in the CCL.

Applying material balances based on standard porous-electrode theory, we have

$$\frac{dN_O^{CCL}}{dz} = \frac{s_O}{n_c F} \frac{dj_c}{dz} \tag{55}$$

where j_c, s_O and n_c are the cathodic current density, the stoichiometric coefficient of oxygen and the number of electrons exchanged in the cathode half-cell reaction, respectively.

2.6.2. Kinetic model for electrochemical oxygen reduction in cathode catalyst layer

The electrochemical reduction of oxygen in this region is described by Tafel kinetics with first-order dependence. Therefore, the cathode current density is given by

$$\frac{dj_c}{dz} = aI_{O,ref}^0 \left[\frac{C_O^{CCL}(z)}{C_{O,ref}}\right] \exp\left(\frac{\alpha_c \eta_c(z) F}{RT}\right) \tag{56}$$

where $aI_{O,ref}^0$ is the cathode volumetric reference exchange-current density, η_c is the cathode overpotential, and α_c is the cathode transfer coefficient.

From Eqs. (55) and (56), the following differential equation can be derived:

$$\frac{d^2 C_O^{CCL}(z)}{dz^2} - \xi^2 C_O^{CCL}(z) = 0 \tag{57}$$

where

$$\xi^2 = \frac{s_O a I_{O,ref}^0}{n_c F D_O^{CCL,eff} C_{O,ref}} \exp(\alpha_c \eta_c F/RT)$$

Solving Eq. (57) with the following boundary conditions:

$$C_O^{CCL} = C_O^{CCL/CBL} \quad \text{at } z = z^{CCL/CBL}$$

$$\frac{dC_O^{CCL}}{dz} = 0 \quad \text{at } z = z^{PEM/CCL}$$

yields an expression for the oxygen distribution in the CCL, namely:

$$C_O^{CCL}(z) = C_O^{CCL/CBL} \frac{\cosh[\xi(z - z^{PEM/CCL})]}{\cosh[\xi \delta^{CCL}]} \tag{58}$$

Integration of Eq. (56) over the cathode catalyst layer gives the cell current density, I, as

$$I^{eff} = \frac{n_c F D_O^{CCL,eff} \xi^2}{s_O} \int_0^{\delta^{CCL}} C_O^{CCL}(z)\, dz \tag{59}$$

where $I^{eff} = I + I^{Cross}$. Thus, the mixed potential effect on the cathode side is taken into account by replacing I by I^{eff}, which is the sum of the electrical current density and the crossed-over current density, I^{Cross}, attributed to the oxidation of crossed-over methanol in the CCL. I^{Cross} can be obtained from Eq. (43) in Section 2.4. As will be shown later, this approach correctly captures the reduction in the open-circuit voltage at high methanol concentrations.

Solving Eqs. (58) and (59) together, I^{eff}, takes the following form:

$$I^{eff} = \frac{n_c F D_O^{CCL,eff} \xi}{s_O} C_O^{CCL/CBL} \tanh(\xi \delta^{CCL}) \tag{60}$$

Eq. (60) can be used to calculate the cathode overpotential for any given cell current density.

2.7. Overall cell voltage

The overall cell voltage is calculated employing the following expression:

$$V = E_{Cell} - \eta_a - \eta_c - I \frac{\delta^{PEM}}{\sigma^{PEM}} \tag{61}$$

where E_{Cell} is the difference between the half-cell potentials of the anode and the cathode corrected for the thermodynamic effects of temperature (T) and pressure (P) as follows:

$$E_{Cell} = E_{Cell}^0 + (T - T_0)\left(\frac{\partial E_{Cell}}{\partial T}\right) - \frac{\Delta N R T}{n_c F} \ln\left(\frac{P}{P_0}\right) \tag{62}$$

where E_{Cell}^0 is the ideal electromotive force under standard conditions of temperature (T_0) and pressure (P_0). $(\partial E_{Cell}/\partial T)$ is the rate of change of E_{Cell} with T and the last term represents the effect of pressure on cathode potential. Since water vapour is assumed to be produced, ΔN is taken to be +0.5. The third term in Eq. (61) represents the overpotential due to ohmic resistance.

3. Results and discussion

The above semi-analytical mathematical model, consisting of several non-linear, coupled algebraic equations, has been solved under galvanostatic conditions (cell current density is fixed to obtain the corresponding cell voltage) using MATLAB® over the range of physiochemical, geometric and kinetic parameters listed in Tables 2a and 2b. Most of these parameters are taken from the literature, as indicated. Transport parameters such as the diffusivity coefficient of methanol in water on the anode side and the binary concentration diffusivity coefficients on the cathode side

Table 2a
Geometric, physicochemical and operating parameters used in the calculations.

Active area of the cell (A)	9 cm^2 [30]
Thickness of the anode backing layer (δ^{ABL})	0.03 cm [30]
Thickness of the anode catalyst layer (δ^{ACL})	0.001 cm (assumed)
Thickness of the membrane (δ^{PEM})	0.01778 cm (Nafion 117)
Porosity of the anode backing layer (ε^{ABL})	0.65 (assumed)
Porosity of the anode catalyst layer (ε^{ACL})	0.4 (assumed)
Thickness of the cathode backing layer (δ^{CBL})	0.03 cm [30]
Thickness of the cathode catalyst layer (δ^{CCL})	0.001 cm (assumed)
Porosity of the cathode backing layer (ε^{CBL})	0.4 (assumed)
Porosity of the cathode catalyst layer (ε^{CCL})	0.3 (assumed)
Air inlet flow rate	600 ml min^{-1} (assumed)
Electrokinetic permeability (k_Φ)	1.13×10^{-15} cm^2 [24]
Hydraulic permeability (k_p)	1.58×10^{-14} cm^2 [24]
Anode kinetic parameter (β)	6.45×10^{-6} (calibration)
Anode kinetic parameter (γ)	3.086×10^{-7} (calibration)
Anode transfer coefficient (α_a)	0.45 (calibration)
Cathode transfer coefficient (α_c)	0.8 [14]
Reference cathode exchange current density ($I_{O,ref}^0$)	3.75×10^{-7} A cm^{-2} (calibration)
Concentration of protons in the membrane ($C_{H^+}^{PEM}$)	1.2×10^{-3} mol cm^{-3} [24]

Table 2b
Temperature dependant physicochemical parameters.

Property (K)	343	348	353	358	363
Diffusivity coefficient of methanol in water D_{Me-W} ($cm^2\ s^{-1}$)	3.3×10^{-5}	4.5×10^{-5}	4.1×10^{-5}	4.5×10^{-5}	5.3×10^{-5}
Diffusivity coefficient of methanol in the membrane D_{Me}^{PEM} ($cm^2\ s^{-1}$)	6.06×10^{-6}	6.72×10^{-6}	7.42×10^{-6}	8.17×10^{-6}	9.0×10^{-6}
Membrane water content λ [25]	15.4	16.0	17.0	17.5	20.0
Viscosity of liquid water, μ ($g\,cm^{-1}\ s^{-1}$)	4.061×10^{-3}	3.8×10^{-3}	3.565×10^{-3}	3.55×10^{-3}	3.165×10^{-3}

are estimated making use of empirical correlations available in the literature. Results from the calculations are discussed below.

3.1. Limiting current for low methanol feed concentrations

For liquid-feed PEM-DMFCs operating with low methanol feed concentrations, limiting current behaviour can be observed at relatively low current densities. This behavior can be attributed to mass-transport limitations of methanol supply to the reactive zones in the anode compartment [29]. Therefore, the limiting current density may be interpreted as the current density that corresponds to zero methanol concentration in the ACL or as the current density at which the flux of methanol through the ABL equals the rate of electrochemical oxidation of methanol in the ACL. This can be seen in Fig. 2 where the predicted variation of methanol concentration in the ABL, ACL and PEM is shown for different current densities and for different methanol feed concentrations. In Fig. 2a, for a methanol feed concentration of 0.125 M at 90 °C and at a methanol feed flow rate of 1.36 ml min^{-1}, the methanol concentration decreases in the ACL as the current density increases and becomes zero at $I = 0.045\ A\,cm^{-2}$. Decreasing methanol concentration with increasing current density can also be observed at the AFC|ABL interface. For feed concentrations 0.125 and 0.5 M, and at the same temperature and methanol feed flow rates, this happens at current densities of 0.093 and 0.197 $A\,cm^{-2}$, respectively (see Fig. 2b and c). It can be seen from these methanol concentration profiles that a higher flux of methanol in the anode catalyst layer cannot be sustained. This constitutes mass-transport limitation on the anode side which limits the current density that can be extracted.

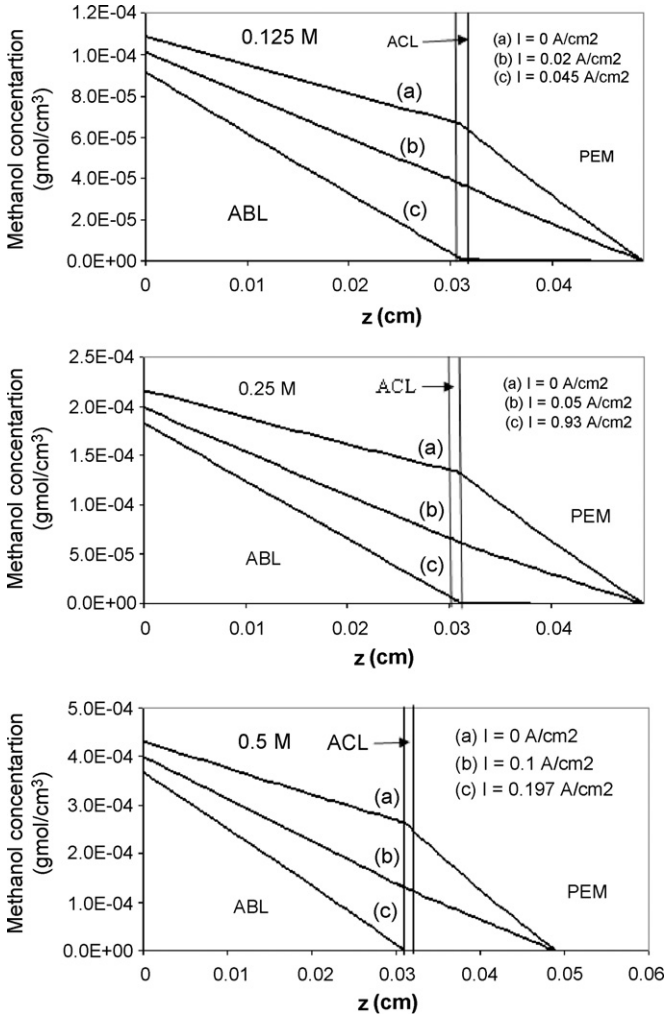

Fig. 2. Predicted methanol concentration profiles in the anode compartment and the PEM regions for a methanol feed concentration of (a) 0.125 M, (b) 0.25 M and (c) 0.5 M at a methanol feed flow rate of 1.36 ml min^{-1} at 90 °C, and at an air feed cathode pressure of 2 bar.

The limiting current densities predicted by the present model for three different methanol feed concentrations (0.125, 0.25 and 0.5 M) at 70 and 90 °C are compared with experimental data taken from literature [10,30] in Fig. 3a and b, respectively. Further comparison of the predicted and the experimental limiting current densities [30] is shown in Fig. 3c as a function of cell operating temperatures for a fixed methanol feed concentration of 0.5 M at a methanol feed flow rate of 1.36 ml min^{-1}. In these experiments, the polarization curve show a sharp drop in the voltage which is due to methanol mass-transport limitations. The current density at which the extrapolated cell voltage tends to zero is taken as the experimentally determined limiting current density and is used for comparison. It can be observed that the limiting current densities increase with increasing methanol feed concentrations (over the range of concentrations used here) and operating temperatures. Increasing limiting current density with increasing cell temperature can be attributed to enhanced methanol mass transport across the anode compartment. A different dependence of methanol feed concentration on limiting current behaviour can be observed with high methanol feed concentrations and this will be discussed later. Since only a single-phase mass transport model is used here, the model cannot be used to predict limiting current densities accurately, if the carbon dioxide produced on the anode side is not in a fully dissolved state.

3.2. Methanol crossover

A non-zero value of methanol concentration at the ACL|PEM interface can lead to methanol crossover through the PEM to the cathode side where it is oxidized without producing usable protons and electrons. It also competes with the oxygen diffusing through the CBL. The mass-transport models developed for the anode compartment and the PEM are used to explore the effect of various parameters on this undesirable methanol crossover phenomenon.

Fig. 4a and b illustrates the current density effects on methanol crossover for various methanol feed concentrations ranging from 0.125 to 5.0 M at 90 and 70 °C, respectively. Decreasing methanol crossover with decreasing temperature can be observed. The effect of temperature on the crossover is related to the methanol diffusivity through the PEM. With all the other parameters remaining the same, decreasing the cell temperature decreases the diffusivity of methanol and thus the crossover flux through the PEM. Fig. 4a and b also show that the dependence of methanol crossover on the cell current density, as a function of methanol feed concentration, is not unique. At low feed concentrations, the crossover flux decreases

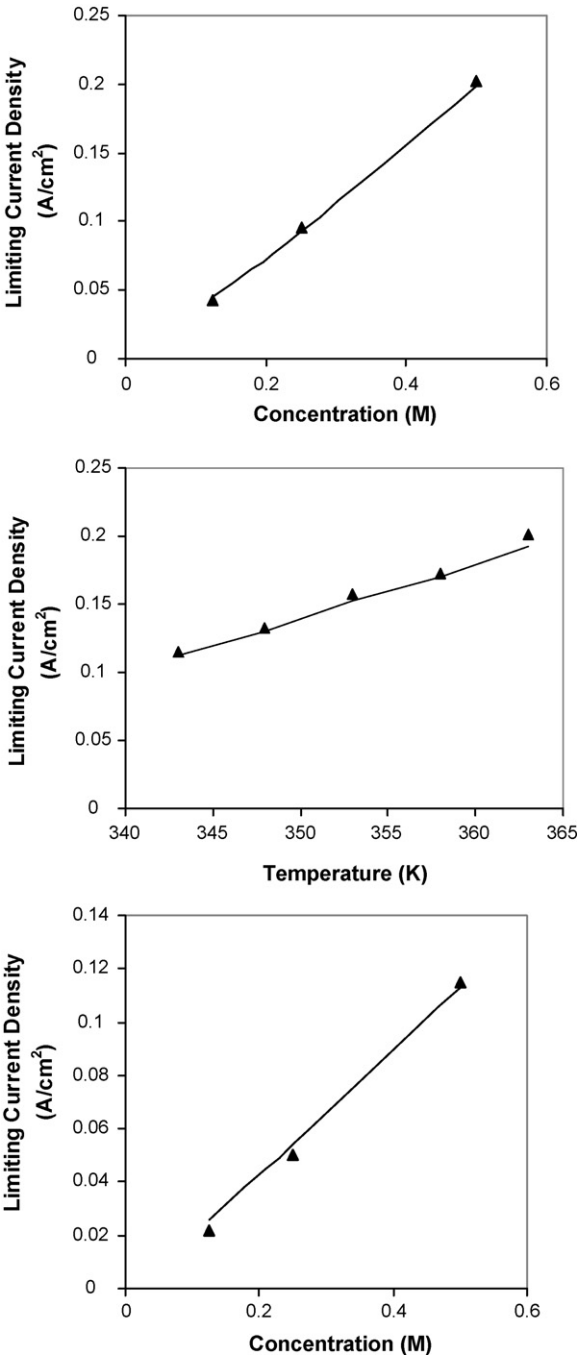

Fig. 3. Limiting current densities predicted using the present mass transport model (solid line) and experimental data (markers) [30] at a methanol flow rate of 1.36 ml min^{-1} for (a) various methanol concentrations at a cell temperature of 90 °C and cathode side pressure of 2 bar, (b) for various cell temperatures at a methanol concentration of 0.5 M and at a cathode side pressure of 2 bar, and (c) for various methanol concentrations for a temperature of 70 °C and cathode side pressure of 3 bar.

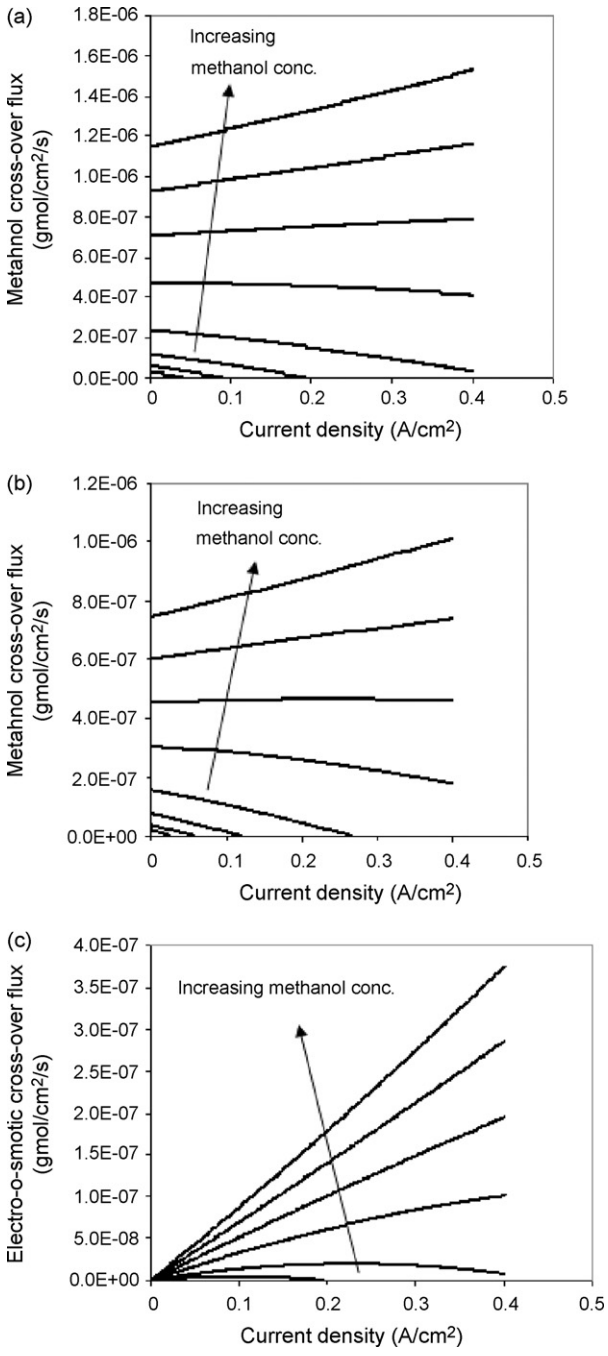

Fig. 4. (a) Predicted methanol crossover flux vs. cell current density for various methanol feed concentrations (0.125, 0.25, 0.5, 1.0, 2.0, 3.0, 4.0, and 5.0 M) at a methanol feed flow rate of 1.36 ml min^{-1}, at 90 °C, and at an air feed cathode pressure of 2 bar. (b) Predicted methanol crossover flux vs. cell current density for various methanol feed concentrations (0.125, 0.25, 0.5, 1.0, 2.0, 3.0, 4.0, and 5.0 M) at a methanol feed flow rate of 1.36 ml min^{-1}, at 70 °C, and at an air feed cathode pressure of 2 bar. (c) Predicted electro-osmotic methanol crossover flux vs. cell current density for various methanol feed concentrations (0.5, 1.0, 2.0, 3.0, 4.0, and 5.0 M) at a methanol feed flow rate of 1.36 ml min^{-1}, at 90 °C, and at an air feed cathode pressure of 2 bar.

as the current density increases. However, as the feed concentration increases, the methanol crossover flux remains almost constant or increases with increasing current density. Thus an optimization needs to be done between increasing current density and decreasing crossover flux.

Methanol crossover across the PEM takes place via diffusion and convection, the latter arising from the driving forces of potential and pressure gradients. For low methanol feed concentrations, the potential gradient driven electro-osmotic methanol crossover flux is very small (see Fig. 4c), and as the current density is increased, the concentration of methanol at the ACL|PEM interface, which predominantly determines the extent of diffusive methanol crossover flux across the PEM, decreases (see Fig. 2) and becomes zero at the limiting current values. Therefore, for low feed concentrations of methanol, the net methanol crossover flux monotonously decreases with increasing current density and becomes zero exactly at the corresponding limiting current density values. This behaviour in turn confirms that, for low methanol feed concentrations, the methanol

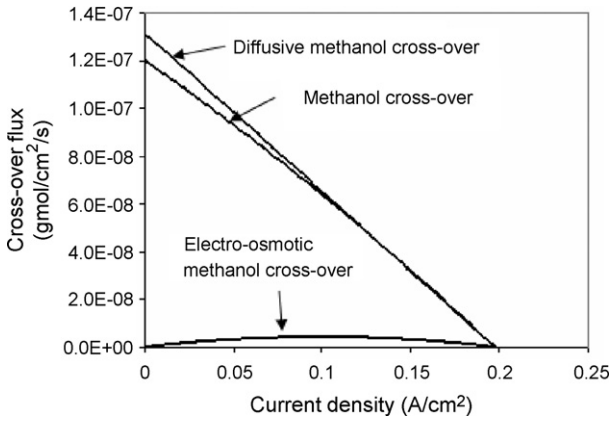

Fig. 5. Predicted diffusive, electro-osmotic, and net methanol crossover flux for a methanol feed concentration of 0.5 M, at a methanol feed flow rate of 1.36 ml min^{-1}, at 90 °C, and at an air feed cathode pressure of 2 bar.

crossover flux across the membrane is purely diffusion-driven (see Fig. 5). However, a lesser net methanol crossover flux than the diffusive crossover flux can be observed up to a current density value of close to 0.1 A cm^{-2}. This is due to the negative effect of pressure gradient driven crossover taking place from the cathode to the anode.

For high methanol feed concentrations, even though the concentration of methanol in the ACL decreases with increasing current density (decreasing diffusive crossover flux can be seen in Fig. 6a),

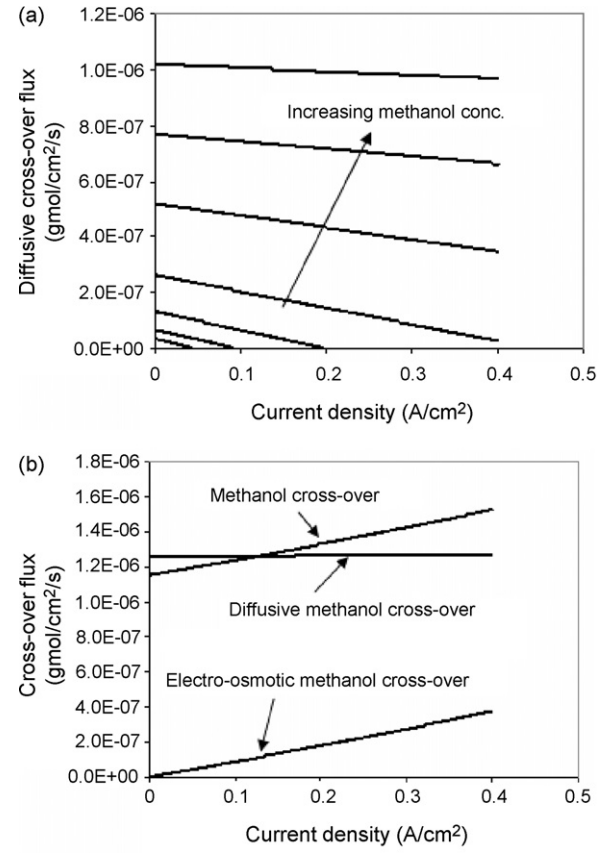

Fig. 6. (a) Predicted diffusive methanol crossover flux vs. cell current density for various methanol feed concentrations (0.125, 0.25, 0.5, 1.0, 2.0, 3.0, 4.0, and 5.0 M) at a methanol feed flow rate of 1.36 ml min^{-1}, at 90 °C, and at an air feed cathode pressure of 2 bar. (b) Predicted diffusive, electro-osmotic, and net methanol crossover flux for a methanol feed concentration of 5.0 M, at a methanol feed flow rate of 1.36 ml min^{-1}, at 90 °C, and at an air feed cathode pressure of 2 bar.

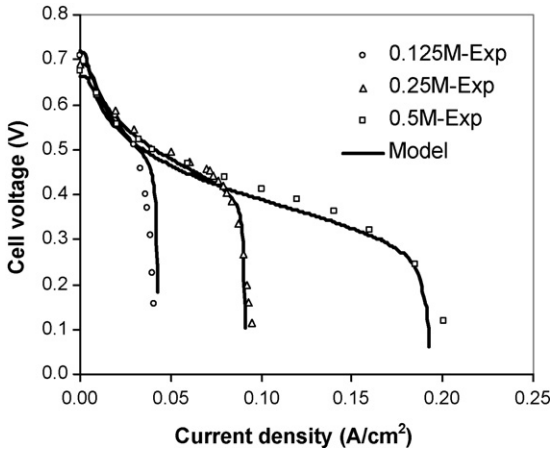

Fig. 7. (a) Cell polarization behavior predicted by the present model (solid lines) and experimental data (markers) [30] for various methanol feed concentrations at a methanol feed flow rate of 1.36 ml min^{-1}, at 90 °C, and at an air feed cathode pressure of 2 bar.

over the range of current densities shown, no significant drop in diffusive crossover flux can be observed. Fig. 6b shows that at a methanol concentration of 5 M, the net crossover flux increases with increasing current density because of the enhanced electro-osmotic crossover flux with increasing current density (Fig. 6b). It is expected that a methanol transport-based limiting current will also be there for high methanol concentrations; but it will be of little practical value. The negative effect of pressure gradient [31] is small and can be observed up to a current density value of 0.1 A cm^{-2}. For 2 and 3 M methanol feed concentrations, the crossover flux remains almost constant and the cell may reach optimum performance with these concentrations with the set of operating conditions used here. The predicted trends are similar to those measured [32] or calculated [11,33,34]. Among the other parameters, the model predictions show that the effect of feed flow rate on methanol crossover is rather slight. However, the thickness of the electrolyte membrane has a significant effect and this is in agreement with the results of Jung et al. [35]. These results show that the Faradaic efficiency (fuel utilization efficiency) of a DMFC is considerably reduced when high current densities (and hence high methanol concentrations) are required.

3.3. Polarization behaviour

3.3.1. Model calibration

In order to predict the polarization curves, the values of the parameters k_1, k_3 and α_a related to the anode kinetics (see Eq.

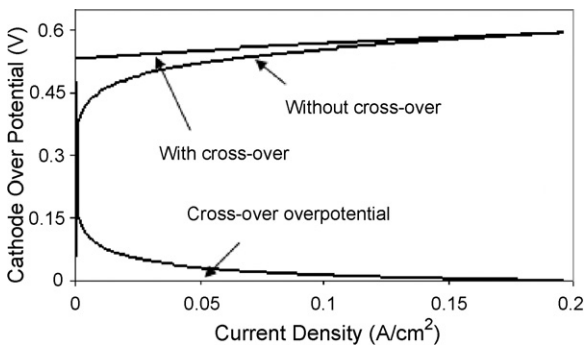

Fig. 8. Effect of methanol crossover on cathode polarization for a methanol feed concentration of 0.5 M at a methanol feed flow rate of 1.36 ml min^{-1}, at 90 °C, and at an air feed cathode pressure of 2 bar.

(33)) are needed. Low-concentration (0.125–0.5 M) data from Ref. [30] have been used to optimize these and are listed in Table 2a. It may be noted that the same set of values of these three anode kinetic parameters have been used for all the results shown in this section. The predicted polarization behaviour for 0.125, 0.25, and 0.5 M methanol feed concentrations is shown in Fig. 7. It can be seen that a good agreement (including for the open-circuit voltage) is observed with the set of transport and kinetic parameters used in this work. Increasing limiting current densities with increasing methanol feed concentrations can also be observed as mentioned previously. Moreover, it is worth noting that the cell voltage goes to zero exactly at the limiting current densities predicted by the mass-transport model. Finally, the effect of increasing methanol concentration on the predicted open-circuit voltage (OCV) is shown in Fig. 7b for concentrations in the range of 0.125–2 M. It can be seen that as the methanol feed concentration increases, the OCV decreases, which is in agreement with experimental data. Further analysis of the predictions shows that this is due to the increased cathode overpotential caused by increased methanol crossover flux.

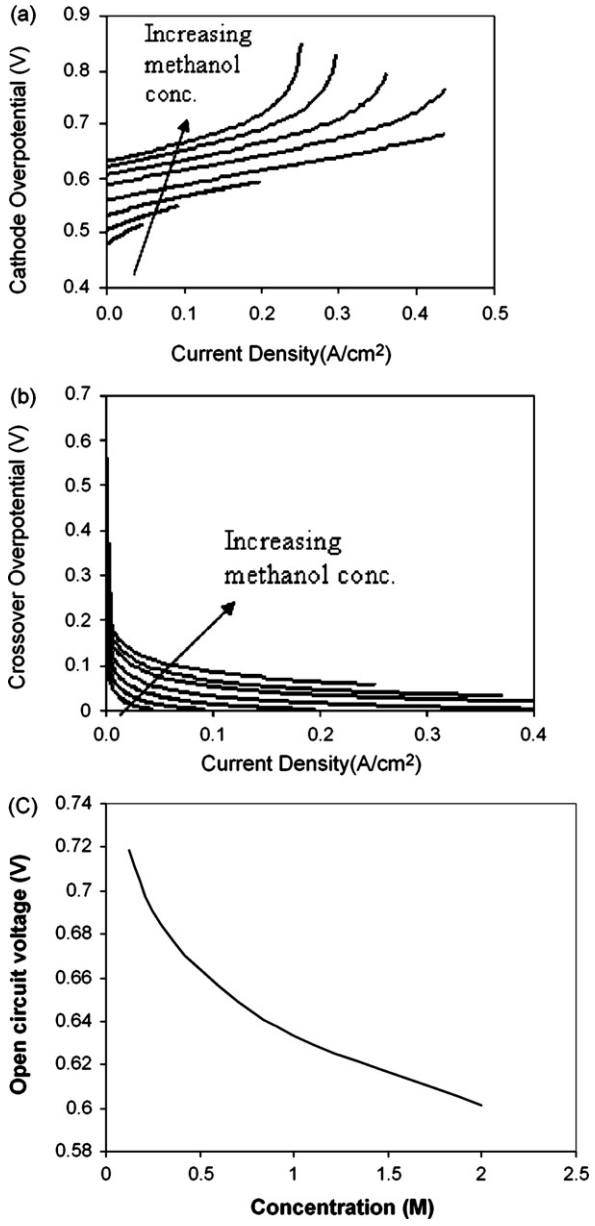

Fig. 9. (a) Predicted cathode polarization behavior for various methanol feed concentrations (0.125, 0.25, 0.5, 1.0, 2.0, 3.0, 4.0, and 5.0 M) at a methanol feed flow rate of 1.36 ml min^{-1}, at 90 °C, and at an air feed cathode pressure of 2 bar. (b) Predicted crossover overpotentials for various methanol feed concentrations (0.125, 0.25, 0.5, 1.0, 2.0, 3.0, 4.0, and 5.0 M) at a methanol feed flow rate of 1.36 ml min^{-1}, at 90 °C, and at an air feed cathode pressure of 2 bar. (c) Predicted open circuit voltages for various methanol feed concentrations (0.125, 0.25, 0.5, 1.0, and 2.0 M) at a methanol feed flow rate of 1.36 ml min^{-1}, 90 °C, and air feed cathode pressure of 2 bar.

3.3.2. *Effect of methanol crossover on polarization behaviour*

The effect of methanol crossover on the cathode overpotential is illustrated in Fig. 8. The difference between the polarization curves with and without crossover indicates the voltage loss caused by methanol crossover or crossover overpotential. As can be seen, methanol crossover results in serious cathode overpotentials at the open-circuit conditions. However, even a very low current density can cause the crossover overpotential to fall sharply which then decreases smoothly with increasing current density.

Fig. 9a, b and c shows, respectively, the predicted cathode overpotential, the crossover overpotential, and the OCV for methanol feed concentrations in the range of 0.125–5 M. Both the overpotentials increase with increasing methanol feed concentration. Of these, the crossover overpotential reduces significantly as the current density decreases while the cathode overpotential remains high and increases drastically at very high methanol concentrations. This is due to the increased mixed-potential effect caused by excessive oxygen consumption by the increased methanol crossover with increasing methanol feed concentrations. The predicted OCV (Fig. 9c) too is dependent on the methanol feed concentration and it decreases from 0.72 to 0.6 V when the feed concentration is increased from 0.125 to 2 M. This trend is consistent with trends reported in the literature. The predicted polarization curves for methanol feed concentrations greater than 0.5 M are plotted in Fig. 10. These show that the limiting current density increases with methanol concentration up to a limit. It then decreases with increasing methanol concentration, which can be attributed to the mixed-potential effect at the cathode. These trends are in good qualitative agreement with reported data [36]. This validates the present treatment of the mixed-potential effect on the cathode side, namely, the use of the effective current density, which is the sum of the actual current density and the equivalent current density required for methanol oxidation, to determine the cathode overpotential (see Eqs. (59) and (60)).

Finally, Fig. 11 illustrates the cell voltage vs. current density characteristics for three methanol feed flow rates. As can be seen, the cell performance is strongly dependent on the methanol feed flow rate only when the flow rates are low. The increase in limiting current density with increasing methanol feed flow rate can be attributed to the increased methanol mass transport across the anode compart-

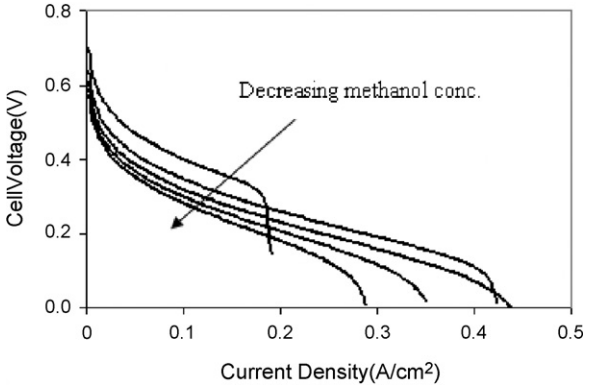

Fig. 10. Predicted cell polarization behavior predicted for higher methanol feed concentrations (1.0, 2.0, 3.0, 4.0, and 5.0 M) at a methanol feed flow rate of 1.36 ml min^{-1}, at 90 °C, and at an air feed cathode pressure of 2 bar.

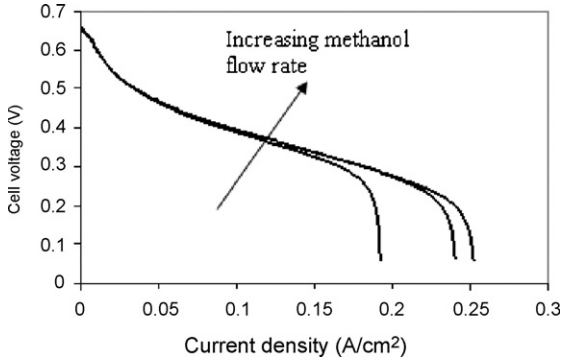

Fig. 11. Predicted polarization behavior for various methanol feed flow rates (1.36, 5.36, and 12.36 ml min^{-1}) for a methanol feed concentration of 1.36 ml min^{-1}, at 90 °C, and at an air feed cathode pressure of 2 bar.

ment. The effect of methanol feed flow rate on methanol crossover is not very significant for high methanol feed flow rates, and the improvements diminish at higher flow rates. These trends are consistent with those reported in the literature [37].

4. Conclusions

A comprehensive one-dimensional, single-phase mathematical model for a liquid-feed polymer electrolyte membrane direct methanol fuel cell (PEM-DMFC) has been developed taking into account all the necessary mass transport and electrochemical phenomena. Diffusion and convective transport of methanol is considered in the ABL, ACL and PEM regions, whereas only diffusional transport of the species is considered on the cathode side. The model also accounts for water transport across the PEM. A multi-step reaction mechanism is considered to obtain a kinetic model to describe the electrochemical oxidation of methanol in the ACL. Tafel type kinetics are used to describe the simultaneous oxygen reduction and electrochemical oxidation of methanol in the CCL. The model fully accounts for the mixed-potential effect caused by methanol crossover at the cathode.

The model predicts well the limiting current behavior (attributed to limiting methanol diffusion on the anode side) at low different low methanol feed concentrations at different operating temperatures. The model is calibrated against experimental polarization curves and good agreement is obtained with other experimental data. It shows that at high methanol feed concentrations, oxygen depletion on the cathode side due to the excessive methanol crossover results in the mass-transport limitations. Thus the loss of efficiency of the DMFC due to fuel crossover at high methanol concentrations is captured well in the model. Further model improvements including multi-phase flow, electronic and protonic potentials, and water and heat management are worth future investigation to improve the predictive capabilities of the present model.

References

[1] C.K. Dyer, Journal of Power Sources 106 (2002) 31–34.
[2] K. Kordesch, G. Simader, Fuel Cells and their Applications, VCH Publishers, Weinsheim, Germany, 1998.
[3] F. Barbir, PEM Fuel Cells: Theory and Practice, Academic Press, New York, 2005.
[4] V. Neburchilov, J. Martin, H. Wang, J. Zhang, Journal of Power Sources 169 (2007) 221–238.
[5] K. Scott, W. Taama, J. Cruickshank, Journal of Power Sources 65 (1997) 159–171.
[6] G.-B. Jung, A. Su, C.-H. Tu, F.-B. Weng, Journal of Fuel Cell Science and Technology 2 (2005) 81–85.
[7] S.F. Baxter, V.S. Battaglia, R.E. White, Journal of Electrochemical Society 146 (1999) 437–447.
[8] K. Scott, P. Argyropoulos, K. Sundmacher, Journal of Electroanalytical Chemistry 477 (1999) 97–110.
[9] A.A. Kulikovsky, J. Divisek, A.A. Kornyshev, Journal of Electrochemical Society 147 (2000) 953–959.
[10] K. Sundmacher, T. Schultz, S. Zhou, K. Scott, M. Ginkel, E.D. Gilles, Chemical Engineering Science 56 (2001) 333–341.
[11] K.T. Jeng, C.W. Chen, Journal of Power Sources 112 (2002) 367–375.
[12] A.A. Kulikovsky, Electrochemistry Communications 5 (2003) 1030–1036.
[13] A.A. Kulikovsky, Electrochemistry Communications 5 (2003) 530–538.
[14] H. Guo, C.-F. Ma, Electrochemistry Communications 6 (2004) 306–312.
[15] Z.H. Wang, C.Y. Wang, Journal of Electrochemical Society 150 (2003) A508–A519.
[16] J. Ge, H. Liu, Journal of Power Sources 160 (2006) 413–421.
[17] J. Ge, H. Liu, Journal of Power Sources 163 (2007) 907–915.
[18] H.A. Gasteiger, N.M. Marković, P.N. Ross, E. Cairns, Electrochimica Acta 40 (1995) 91–98.
[19] P.S. Kauranen, E. Skou, Journal of Electroanalytical Chemistry 404 (1996) 1–13.
[20] W.H. Lizcano-Valbuena, V.A. Paganin, E.R. Gonzalez, Electrochimica Acta 47 (2002) 3715–3722.
[21] T. Vidakovic, M. Christov, K. Sundmacher, Journal of Electroanalytical Chemistry 580 (2005) 105–121.
[22] H.A. Gasteiger, N.M. Marković, P.N. Ross, E. Cairns, Journal of Physical Chemistry 97 (1993) 12020–12029.
[23] J.P. Meyers, J. Newman, Journal of Electrochemical Society 149 (2002) A718–A728.
[24] D.M. Bernardi, M.W. Verbrugge, Journal of Electrochemical Society 139 (1992) 2477–2491.
[25] J.T. Hinatsu, M. Mizuhata, H. Takenaka, Journal of Electrochemical Society 141 (1994) 1493–1498.
[26] R.B. Bird, W.E. Stewart, E.N. Lightfoot, Transport Phenomena, Wiley International Edition, John Wiley & Sons, Inc., USA, 1960.
[27] P.D. Nuefeld, A.R. Jansen, R.A. Aziz, Journal of Chemical Physics 57 (1972) 1100–1102.
[28] R.E. Treybal, Mass Transfer Operations, International Edition, McGraw-Hill, Singapore, 1981.
[29] K. Scott, W. Taama, S. Kramer, P. Argyropoulos, K. Sundmacher, Electrochimica Acta 45 (1999) 945–957.
[30] K. Scott, W. Taama, P. Argyropoulos, K. Sundmacher, Journal of Power Sources 83 (1999) 204–216.
[31] J. Cruickshank, K. Scott, Journal of Power Sources 70 (1998) 40–47.
[32] H. Dohle, K. Wippermann, Journal of Power Sources 135 (2004) 152–164.
[33] B.L. Garcia, V.A. Sethuraman, J.W. Weidner, R.E. White, R. Dougal, Journal of Fuel Cell Science and Technology 1 (2004) 43–48.
[34] J.P. Meyers, J. Newman, Journal of Electrochemical Society 149 (2002) A729–A735.
[35] D.H. Jung, C.S. Lee, C.S. Kim, D.R. Shin, Journal of Power Sources 71 (1998) 169–173.
[36] J. Ge, H. Liu, Journal of Power Sources 142 (2005) 56–69.
[37] J. Han, H. Liu, Journal of Power Sources 164 (2007) 166–173.